

H₂O₂-assisted Sonophotocatalytic Degradation of Diclofenac using a Visible Light-Active Flower-like Micron-sized TiO₂ Photocatalyst

Thamisha Steven¹, Rab Nawaz^{1,2}, Nurul Tasnim Sahrin^{1,2}, Kar Mun Lee^{1,2},
Claudia L. Bianchi³ and Chong Fai Kait^{1,2*}

¹Fundamental and Applied Sciences Department (FASD), Universiti Teknologi PETRONAS, 32610 Seri Iskandar, Perak, Malaysia

²Centre of Innovative Nanostructures & Nanodevices (COINN), Institute of Autonomous System, Universiti Teknologi PETRONAS, 32610 Seri Iskandar, Perak, Malaysia

³Università degli Studi di Milano, Dipartimento di Chimica, via Golgi, 19 – 20133 Milano, Italy

*Corresponding author (e-mail: chongfaikait@utp.edu.my)

The recovery of TiO₂ nanoparticles after utilization is a major challenge that hinders the wide-scale implementation of photocatalytic technology in wastewater treatment. In this study, an easily recoverable flower-shaped micron-sized TiO₂ (MST) photocatalyst was synthesized from nano-sized TiO₂ seeds via a hydrothermal process. The synthesized MST photocatalyst displayed an average particle size of 1.577 μm with 2.7 eV bandgap energy and 100.18 m²/g surface area. The photocatalytic performance of the synthesized material was evaluated for the degradation of diclofenac (DCF) from aqueous solution under visible light. The degradation efficiency under visible light reached 52.87% in 120 min. When photocatalysis was coupled with ultrasonication (US), namely sonophotocatalysis, the DCF degradation efficiency increased to 62.61%. The highest DCF degradation efficiency (86.92%) was achieved under the optimized conditions of 30 kHz US frequency, 0.4 g/L of TiO₂ loading, 10 ppm initial concentration of DCF, and 1.0 mM H₂O₂ dosage. The synergy index of sonophotocatalysis was 1.25, indicating the synergistic effects of both sonocatalysis and photocatalysis on DCF degradation efficiency. The MST photocatalyst was easily recovered through centrifugation after reaction and reused for another two cycles of sonophotocatalysis. The photocatalyst was significantly stable under these process conditions, with only a 5.19% decrease in degradation after three consecutive cycles.

Key words: Diclofenac degradation; micron-sized TiO₂; ultrasonication; photocatalysis; sonophotocatalysis; synergy index

Received: March 2021; Accepted: June 2021

Diclofenac (DCF) is a non-steroidal anti-inflammatory drug used to treat fever, pain, and arthritis. It has been detected in the μg/L range in drinking water, ground water and surface water all around the world [1-3]. Its occurrence in water resources can cause harmful effects on aquatic organisms, human health, and the ecosystem. For instance, DCF can cause cytopathological symptoms in the gills, kidneys, and liver of rainbow trout [4]. One of the most crucial ecological impacts of DCF residues is the decline in vulture populations [5]. DCF is considered persistent due to its stable chemical structure [6] and cannot be removed effectively by conventional wastewater treatment approaches. Therefore, it is essential to develop more effective and sustainable treatment technologies for the removal of DCF from pharmaceutical wastewater to safeguard the ecosystem and human health.

Recently, various advanced oxidation processes (AOPs) including electrochemical oxidation, photocatalysis, photo-Fenton and ultraviolet/H₂O₂ [7, 8] have been investigated for their effects on the degradation of DCF from wastewater.

Photocatalysis based on TiO₂ nanomaterials coupled with other AOPs such as UV/H₂O₂ and ultrasonication (US) has been touted as the most promising approach for the degradation of organic pollutants [9, 10]. Photocatalysis assisted by US is a more consolidated approach to improve the degradation of pollutants as cavitation can enhance the performance of photocatalysis via the promotion of mass transfer and production of additional radicals, which are the predominant species taking part in photoreactions. In addition, US helps in the continuous regeneration of the photocatalyst surface, exposing active sites for DCF adsorption and therefore leading to higher photodegradation activity. For example, Meroni et al. [8] reported an enhanced degradation of DCF by combining UV/TiO₂/US processes. Similar results of enhanced DCF degradation were also reported by Madhavan et al. [11] using three different photocatalysts including Fe-ZnO, TiO₂ and ZnO. It is important to note that UV light was the energy source employed for the reactions. Although UV light is better in producing high reaction rates in the oxidation of organic compounds, it represents only 5% of solar irradiation. In contrast, visible light accounts for 45%

of sunlight [12], making it a more attractive choice in the long run.

Both micron- and nano-sized TiO₂ have been utilized to improve the degradation efficiencies of pollutants in water treatment and air pollution control [13]. TiO₂ has been commonly used in suspension form due to its simplicity and superior degradation efficiency. The degradation efficiency of TiO₂ in suspended photoreactors (PRs) is higher compared to the immobilized form because of the greater mass transfer rate of reactants and higher specific surface area to reactor volume ratio [14]. Nevertheless, the nanophotocatalyst dispersed in suspended PRs needs to be removed or recovered from the reaction media because effluent containing nanomaterials can be toxic and harmful to living organisms. Clement, Hurel and Marmier [15], studied the acute and chronic toxicity of TiO₂ nanoparticles on daphnia, algae, rotifers and plants as model organisms. Their results revealed that a TiO₂ photocatalyst in the anatase form is toxic. Furthermore the nanosized materials when accumulated in the human body may cause genotoxicity, chronic inflammation, organ failure or carcinogenicity [16]. The problems related to TiO₂ nanoparticles (size < 100 nm) include inhalation and skin interaction of particles so tiny that the human body's barriers may not recognize them. Thus, recovery or separation of the nanophotocatalyst is one of the crucial factors to be considered for practical application of TiO₂-based technology for DCF degradation. An alternative to TiO₂ nanoparticles is to synthesize micron-sized TiO₂ (MST) and compare its performance in the degradation of diclofenac in pharmaceutical wastewater. The main advantage of MST over nanoparticles is that microparticles employed for the treatment of wastewater can be separated easily after utilization whereas the separation of nanoparticles involves tedious procedures [8, 17]. The separation of nano-sized TiO₂ requires energy-intensive processes such as ultrafiltration or nanofiltration [18] which are costly. In addition, the use of MST reduces the risk of inhalation during deployment. On the other hand, about 50% of nanometric TiO₂ atoms are present on

the surface and due to their extreme sensitivity, structural failure occurs frequently on its surface [13]. As shown in Table 1, most previously reported studies utilized commercially available MST (Kronos 1077) for the degradation of environmental pollutants. For instance, Bianchi et al. [17] investigated the degradation of volatile organic compounds using Kronos 1077 and reported 100%, 100%, and 46% degradation of acetone, acetaldehyde, and toluene within 90, 70, and 360 min respectively, under UV irradiation. Other pollutants investigated were basic orange, phenol, methylene blue, bisphenol A and methyl orange using MST synthesized via hydrothermal, sol gel or a combination of sol gel-hydrothermal and sol gel-anodization processes [18-23]. To date, there seems to be limited work on MST with a reduced bandgap deployed for the degradation of DCF under a visible light source.

The main aim of the present study was to develop a visible light-active MST photocatalyst for sonophotocatalytic treatment of pharmaceutical wastewater contaminated with diclofenac. In order to achieve the main goal, MST was grown from coloured TiO₂ nanoparticles synthesized in our previous work [24] to obtain micrometric scale TiO₂ with flower-shaped morphology. The performance of the synthesized flower-shaped MST was assessed via different AOPs (photolysis, sonolysis, sonophotolysis, sonocatalysis, photocatalysis, sonophotocatalysis) for DCF removal. The effects of different operational parameters such as initial concentration of DCF, MST loading, and H₂O₂ dosage on DCF removal was also thoroughly investigated. Kinetics studies and reusability tests were also conducted to determine the order of the reactions, stability, and recovery of the MST photocatalyst. The novelty of the present research is related to the use of coloured TiO₂ nanoparticles to synthesise a high surface area flower-shaped micron-sized TiO₂ (MST) which is visible light-active and can be recovered easily after photodegradation of DCF. To our knowledge, the synthesis and application of a flower-shaped MST has not been reported by other research groups in photocatalysis or sonophotocatalysis.

Table 1. Recent studies on the synthesis of MST photocatalysts employed for photocatalytic oxidation of various pollutants.

Synthesis method	Target pollutant	Concentration (mg/L)	Particle size (µm)	Degradation efficiency (%)	Ref.
Commercial TiO ₂ (Kronos 1077)	Diclofenac	25	---	100	[8]
Commercial TiO ₂ (Kronos 1077)	Acetone	400	0.1	100	[17]
Commercial TiO ₂ (Kronos 1077)	Acetaldehyde	400	0.1	100	
Commercial TiO ₂ (Kronos 1077)	Toluene	400	0.1	46	
Sol-gel/hydrothermal	Basic orange 2	50	3–14	76	[18]
Sol-gel cum anodization	Phenol	10	1.0	60	[19]
Hydrothermal	Methylene blue	50	2–3	100	[20]
Sol-gel	Bisphenol A	20	3–5	99.7	[21]
Hydrothermal	Methyl orange	20	---	100	[22]
Hydrothermal	Methylene blue	40	1	52	[23]

EXPERIMENTAL

1. Materials

Diclofenac sodium (98%) was purchased from Alfa Aesar, (USA) while hydrogen peroxide (H₂O₂, 30%), sodium hydroxide (NaOH, 99.9%), and hydrochloric acid (HCl, 37%) were purchased from Merck (Darmstadt, Germany) and used as received. The coloured TiO₂ nanoparticles synthesized in our previous work [24] were used as the starting material for the synthesis of the MST photocatalyst. Deionized (DI) water was used throughout the experiments.

2. Synthesis of Micron-sized TiO₂ Photocatalyst

The micron-sized TiO₂ (MST) photocatalyst was synthesized from coloured nano-sized TiO₂ [24] via a modified hydrothermal technique reported by Jitputti et al. [25]. Specifically, 0.2 g of the TiO₂ nanoparticles were suspended in 20 mL of 10 M NaOH solution followed by vigorous stirring to achieve homogeneity. The mixture was transfer to a 100 mL Teflon-lined autoclave and hydrothermally treated at 125°C for 24 h in an oven (Mettler GmbH + Co.KG). The obtained material was rinsed with DI water before being immersed in HCl (pH 2) for 24 h, rinsed again with DI water and dried at 40°C for 24 h in an oven. Finally, the MST photocatalyst was produced after calcination at 500°C for 2 h in a muffle furnace (Nabertherm, Lilienthal, Germany).

3. Characterization of Micro-sized TiO₂ Photocatalyst

The X-ray diffraction (XRD) pattern of the synthesized MST was recorded using an X-ray diffractometer (PANalytical X'Pert³ Powder, AA Almelo, The Netherlands) to identify its crystalline structure. The XRD pattern was acquired at room temperature using CuK_α irradiation between 20° to 80° (2θ) with a step size of 0.001°. Transmission electron microscopy (TEM) images were captured to determine the morphology and average particle size of the synthesized MST using a Hitachi HT7830. FTIR was conducted to identify the functional groups present in the MST. A small amount of the photocatalyst was placed on the sample holder and scanned from 4000 to 400 cm⁻¹ using a Perkin Elmer Frontier 01 spectrophotometer. The diffuse reflectance UV-Visible (DRUV-Vis) spectrum of the photocatalyst sample was obtained using a UV-Vis spectrometer (Agilent Carry100, Santa Clara, CA, USA) with Spectralon as the reference material. The physisorption isotherm of the sample was acquired using a Micromeritics ASAP 2020 analyzer (Micromeritics Corps., Norcross, GA, USA). The sample was degassed at 300°C for 12 h to remove the impurities and moisture from the surface of the sample prior to measurement. The specific surface area of the sample was calculated based on the Brunauer, Emmett and Teller (BET) method from the

adsorption measurement at relative pressures ranging from 0.05 to 0.30. The pore size distribution of the sample was determined using the Barrett-Joyner-Halenda (BJH) method. The properties of the coloured nano-sized TiO₂ used for the synthesis of the flower-shaped MST were also compared.

4. Reaction Performance

4.1. Experimental Setup

Various advanced oxidation processes (AOPs) such as photolysis, sonolysis, sonophotolysis, sonocatalysis, photocatalysis, and sonophotocatalysis were tested for the degradation of DCF from aqueous solution using the experimental set up shown in Figure 1. A 500 W halogen lamp, used as the visible light source, was positioned horizontally at a constant distance of 21 cm from the photoreactor. An ultrasonic processor (UP100H, Hielscher Ultrasonics) with a constant frequency of 30 kHz was fitted with a 3-mm diameter standard sonotrode tip with 460 Wcm⁻² acoustic power density. Pulsed sonication (5s) was used to generate US cavitation bubbles. A magnetic stirrer bar was used to keep the photocatalyst suspended in the DCF suspension. Water was continuously circulated through the jacketed photoreactor to maintain the reaction temperature at 25°C. All experiments were carried out in a jacketed 250-mL Pyrex® cylindrical photoreactor with a working volume of 120 mL DCF solution.

4.2. DCF Degradation Reactions

DCF aqueous solution was treated with different AOPs including photolysis, sonolysis, sonophotolysis, sonocatalysis, photocatalysis, and sonophotocatalysis. For sonocatalysis, photocatalysis and sonophotocatalysis, a specific amount of MST photocatalyst was suspended in the DCF solution to cater for 0.1 g/L of photocatalyst loading. The suspension was vigorously stirred for 30 min in the dark to achieve adsorption-desorption equilibrium of DCF on the photocatalyst surface. The suspension was then irradiated with visible light for 120 min. For sonolysis, only US was carried out while for photolysis, only visible light was used, both conducted in the absence of a photocatalyst.

An aliquot of 2 mL was withdrawn from the reaction medium at specific time intervals of 15, 30, 45, 60, and 120 min using a high precision syringe. The samples were filtered through a 0.22 μm nylon syringe filter and analyzed using UV-Vis spectroscopy (Agilent Cary 60 UV-Vis). The concentration of DCF was monitored at 276 nm [18], and the degradation efficiency of DCF was calculated using Eq. 1.

$$\text{DCF degradation (\%)} = \frac{C_o - C_t}{C_o} \times 100\% \quad (1)$$

where C_o and C_t are the initial DCF concentration and concentration of DCF at a specific time (t), respectively.

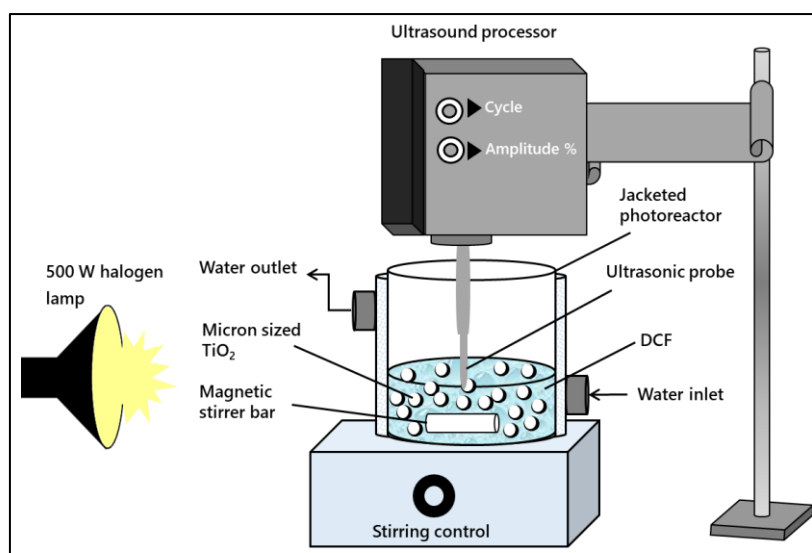


Figure 1. Experimental set up for DCF degradation using various AOPs.

Once the right combination of different processes giving the best performance was confirmed (sonophotocatalysis, photocatalysis combined with sonolysis), the effect of various operational parameters on the DCF degradation efficiency was evaluated. Independent parameters such as initial concentration of DCF (10, 15, 20, and 25 ppm), MST loading (0.1, 0.2, 0.4, 0.6, 0.8, and 1.0 g/L), and concentration of H₂O₂ (0.2, 0.5, 1.0, 5.0, and 10.0 mM) on the sonophotocatalytic degradation of DCF were investigated and optimized. The parameter ranges selected in the present work were previously identified by various authors [26, 27]. In addition to that, the MST was also investigated for recyclability under the optimized process parameters for sonophotocatalysis. After performing DCF removal, the MST photocatalyst was recovered from the reaction medium through centrifugation at 6000 rpm for 10 min at 25°C, washed several times with DI water and reused for the next cycle of DCF removal using fresh 10 ppm diclofenac solution under the same reaction conditions. This process was repeated for another cycle.

RESULTS AND DISCUSSION

1. Characterization of the Synthesized Material

X-ray diffraction (XRD) patterns of the synthesized MST photocatalyst were obtained and compared with the coloured nano-sized TiO₂ starting material to determine the effect of hydrothermal and HCl treatment on its structural properties. The XRD patterns of the micron-sized and nano-sized TiO₂ photocatalysts are shown in Figure 2. Both photocatalysts display characteristic peaks indicating a solely anatase crystalline structure. The diffraction peaks detected at $2\theta = 25.30^\circ, 37.81^\circ, 48.14^\circ, 53.95^\circ, 55.33^\circ, 68.83^\circ$ and 70.34° were assigned to the (101), (004), (200), (105), (211), (204), (116), (220), and (215) planes of the anatase phase, respectively. No

diffraction peaks consistent with rutile or brookite were detected in the diffraction patterns of the micron- and nano-sized TiO₂ photocatalysts, which is in good agreement with previous work [28]. Since MST was grown from the nano-sized TiO₂ by hydrothermal treatment at 125°C for 24 h followed by HCl treatment, its XRD pattern confirmed that the hydrothermal and HCl treatments have no effect on its crystalline structure.

The anatase phase of TiO₂ has been found to display the most favourable properties for photocatalytic reactions, especially in wastewater decontamination, due to the increase in oxidation power of electrons and the ease of electron transfer from the surface of anatase TiO₂ to the adsorbed molecules [29, 30]. The average crystallite sizes of the TiO₂ photocatalysts were calculated using data obtained from the dominant peak at $2\theta = 25.30^\circ$ employing the Scherrer equation (Eq. 2).

$$D = \frac{K\lambda}{\beta \cos\theta} \quad (2)$$

where K is the Scherrer's constant (0.9), λ is the x-ray wavelength of CuK $_{\alpha}$ (0.15418 nm), β is line broadening at half the maximum intensity (radians) and θ is the Bragg's angle (degree). The average crystallite size of the MST was 9.17 nm which was smaller compared to the crystallite size of nano-sized TiO₂ particles (50.87 nm). The peak intensity of the MST was lower compared to nano-sized TiO₂, indicating the MST sample had a lower degree of crystallinity.

Transmission electron microscopy (TEM) analysis was performed to obtain complementary information related to the structural properties and surface morphology of the MST particles. The TEM images of the MST particles, presented in Figure 3(a), display a hierarchical flower-like morphology with closely-packed petals budding from the center of the

receptacles forming a 3-dimensional microstructure. On the other hand, the nano-sized TiO₂ displayed spherical shaped particles as shown in Figure 3(b), a completely different morphology compared to its micron-sized counterparts, indicating that the

hydrothermal and HCl treatment had a significant effect on the size, growth and morphology of the product [17]. The special flower-like morphology is expected to improve the stability of the MST particles and enhance its photocatalytic activity.

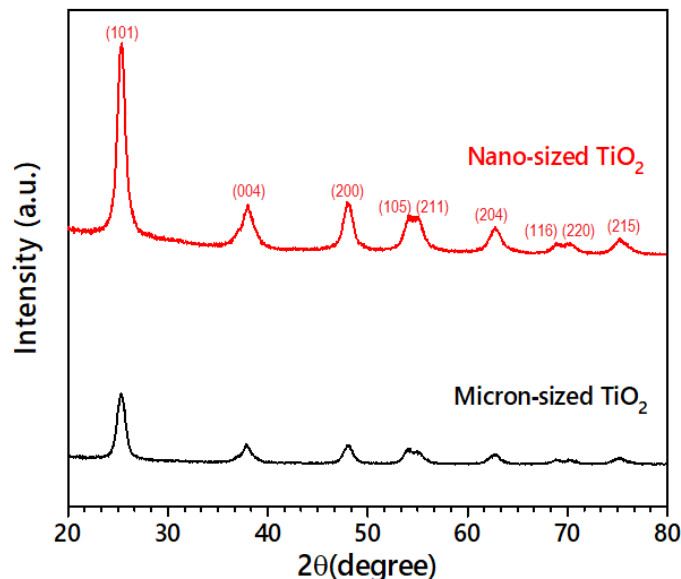


Figure 2. XRD patterns of the synthesized micron-sized and nano-sized TiO₂ particles.

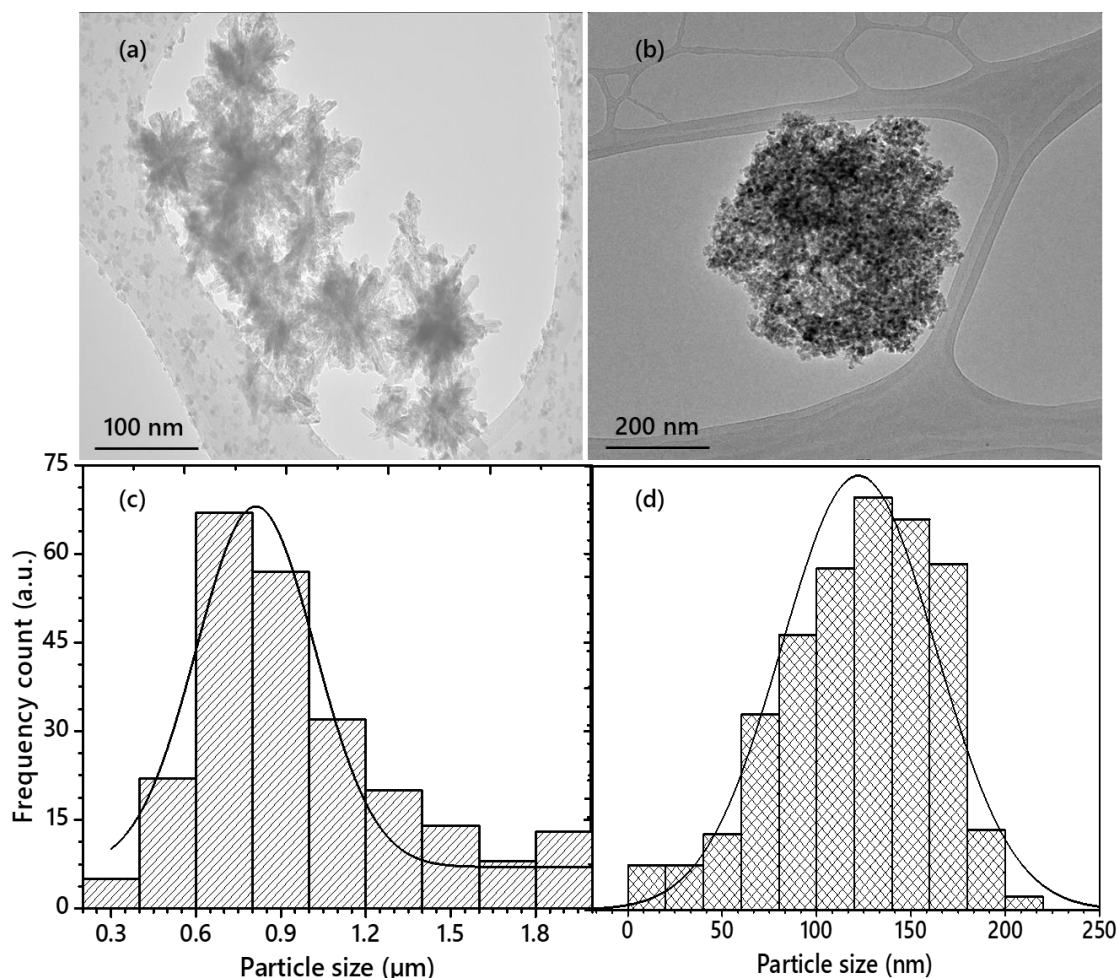


Figure 3. TEM images of (a) MST particles and (b) nano-sized TiO₂ particles, and particle size distributions of (c) MST particles and (d) nano-sized TiO₂ particles.

The particle size distribution of the micron-sized and nano-sized TiO₂ particles was estimated by measuring the diameter of 100 randomly selected particles from magnified TEM images [Figure 3(a & b)] using Image J software. A similar approach was also reported by Yahaya et al. [31]. The particle size distribution of the synthesized micron-sized and nano-sized TiO₂ was calculated based on a Gaussian fitting as presented in Figures 4(c) and (d), respectively. Most of the particles of MST were in the range of 0.5–1.5 μm with an average particle size of 1.577 μm as presented in Figure 3(c). The range was wider compared to Kronos 1077, a commercial micrometric TiO₂ with particle sizes ranging from 100–150 nm [8]. On the other hand, the nano-sized TiO₂ particles were mainly distributed in the range of 5–200 nm with an average particle size of 122 nm as displayed in Figure 3(d).

Figure 4(a) compares FTIR spectra of the micron-sized and nano-sized TiO₂ particles. Both samples display a broad band at 3233.40 cm^{-1} attributed to the O–H stretching while the peak at 1621.57 cm^{-1} was correlated to H–O–H bending. These peaks may represent physically-adsorbed water. The broad band observed at 666.87 cm^{-1} corresponds to Ti–O stretching.

The DRUV-Vis spectra of the micron-sized and nano-sized TiO₂ are shown in Figure 4(b). The maximum absorption edge of MST was located at 547.6 nm, indicating a higher diffuse reflectance capability and better visible light absorption. Compared to nano-sized TiO₂, MST shows enhanced visible-light absorption which can accelerate electron-hole pair separation. As it is well established that the photoactivity of TiO₂ depends on the number of working electrons and holes on its surface, the amount of charge carriers depends on light absorption [32]. In other words, the more light is absorbed by TiO₂, the greater the number of working electrons and holes that are segregated on the surface, and the higher the photoactivity. The enhanced visible light absorption by MST may be attributed its special flower-like structure since such morphology improves visible-light harvesting capability and facilitates efficient transport of charge carriers to the surface of the photocatalyst [33]. As observed in the inset of Figure 4(b) the bandgap energy calculated from Tauc's plot was significantly reduced to 2.71 eV for MST compared to nano-sized TiO₂ (2.96 eV). The commercial Degussa P25 TiO₂, which is not visible light-active, has its bandgap at 3.20 eV.

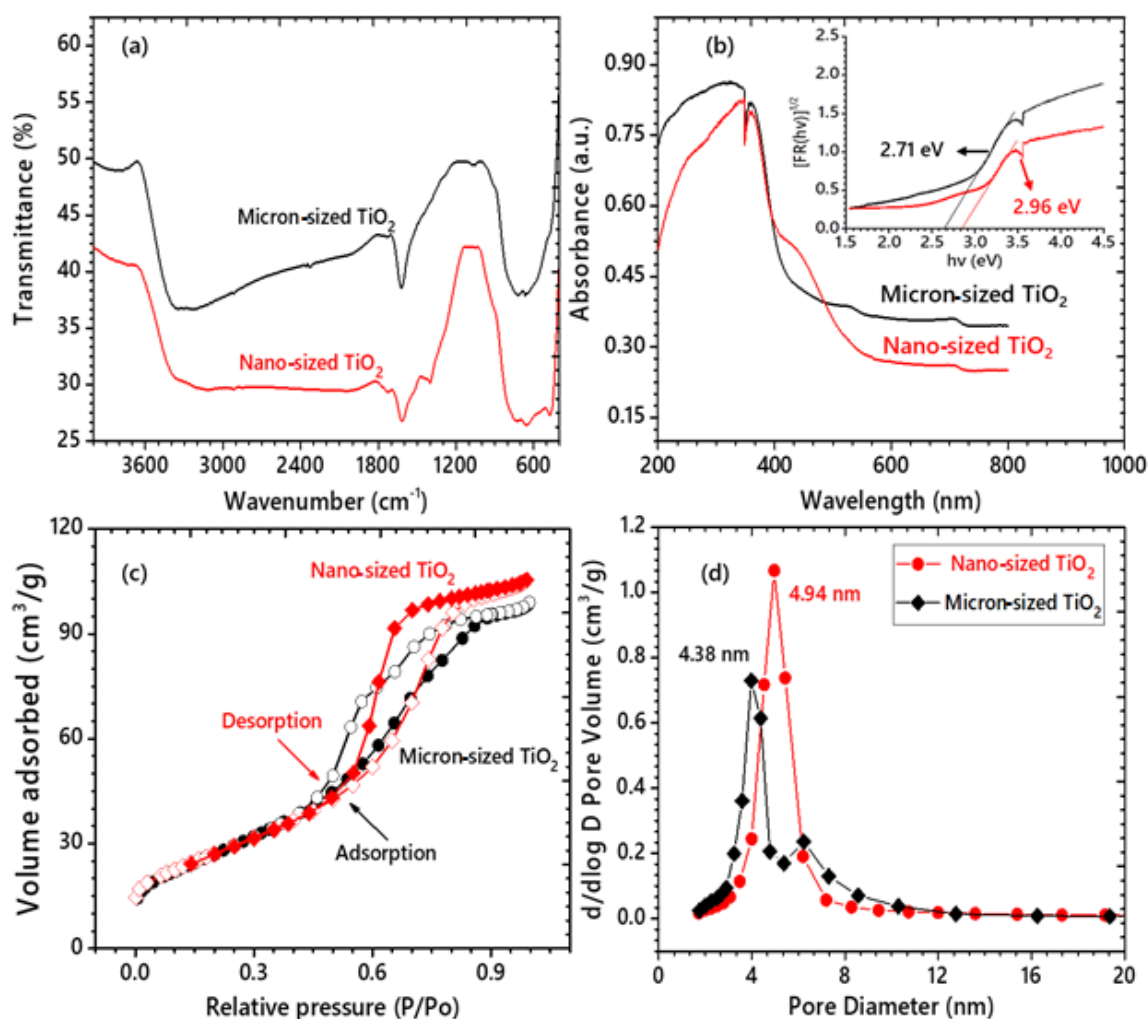


Figure 4. (a) FTIR spectra, (b) DRUV-Vis spectra (inset: Tauc's plot), (c) Nitrogen adsorption-desorption isotherms, and (d) pore size distribution of TiO₂ photocatalysts.

Table 2. Properties of the synthesized MST photocatalyst compared to nano-sized TiO₂.

Property	Unit	Micron-sized TiO ₂	Nano-sized TiO ₂ ^a
Crystallite size	nm	9.17	—
Average particle size	μm	1.577	16–22 nm
Specific surface area	m ² /g	100.18	99.88
Average pore volume	cm ³ /g	0.157	0.161
Average pore size	nm	4.38	4.94
Band gap	eV	2.71	2.96
Absorption edge wavelength	nm	457.62	>400

Sourced from Nawaz et al. [24].

The nitrogen physisorption isotherms of micron-sized and nano-sized TiO₂ particles are presented in Figure 4(c). The textural analysis indicates that the micron-sized and nano-sized TiO₂ particles are mesoporous, displaying type IV isotherms with a H₂ hysteresis loop. The hysteresis loop shows a plateau in the desorption branch at high relative pressure which is typical of mesoporous material with a small pore size distribution. A steeper desorption branch at high relative pressure was observed. This shows that the mesoporous micron-sized and nano-sized TiO₂ have small pore size distributions [34]. The hydrothermal and HCl treatment did not show any significant effects on the textural properties of the MST. Multipoint BET specific surface area, pore volume and pore size data for micron-sized TiO₂ are presented in Table 2. The MST showed a specific surface area of 100.18 m²/g, which is comparable to nano-sized TiO₂ (99.88 m²/g) and 50% higher compared to commercial P25 (50.81 m²/g). The initial spherical morphology of the nano seeds was converted to high surface area flower-shaped micron-sized materials. These results are consistent with previously reported studies where the surface area of untreated TiO₂ was comparable to that of hydrothermally treated TiO₂ at 90°C for 10 h [20]. In contrast, Wei et al. [35] has reported a small increase in surface area from 50 m²/g to 66.5 m²/g during hydrothermal treatment at 160°C for 2 h. Studies suggested three stages of crystallite growth and evolution of TiO₂ morphology during hydrothermal treatment. The second stage (2–5 h), where Ti is gradually released from the bulk, plays a unique role in TiO₂ nucleation and growth that leads to different morphologies such as nanocones, bipyramids, and spherical shaped particles [36].

It has been reported that TiO₂ nanoparticles had higher surface areas after hydrothermal treatment [37]. More importantly, the synthesized MST showed the formation of cylindrical pores. Formation of pores with different morphology clearly demonstrates the

role of either the glycerol used during the synthesis of nano-sized TiO₂ particles or the hydrothermal treatment during the synthesis of MST in engineering the pore structure, as titania is otherwise known to form ink-bottle type pores in the absence of structure-directing agents [38]. A comparison of the pore size distribution of micron-sized and nano-sized TiO₂ is displayed in Figure 4(d). The mean pore size of the MST was determined to be 4.38 nm while that of the nano-sized particles was 4.94 nm, showing a decrease in the pore size of the MST. Interestingly, it becomes clear that glycerol plays an important role in forming the pore structures whereas hydrothermal treatment leads to an evolution of the pore structures from mono-modal to bimodal pore size distribution as indicated by the presence of two peaks in the pore size distribution curve for MST. It was thought that more micelles induced by hydrothermal treatment may be one of the possible reasons for the formation of secondary pores (bimodal shape) [39, 40]. It can be concluded that the hydrothermal treatment not only increased the particle size of TiO₂ from nanometer spheres to micrometer flower-shape particles, but it also seems to be a promising approach for developing exciting architectures of bimodal microstructures of TiO₂, which may possess improved properties for enhanced organic pollutant adsorption and subsequent degradation [41].

2. Diclofenac Degradation Using Different AOPs

The diclofenac (DCF) degradation efficiencies of model wastewater using various AOPs are displayed in Figure 5(a). The objective of the combination of AOPs is to enhance the degradation of DCF that is not achievable with single process under the same set of experimental conditions. Photolysis managed to achieve only 8.62% DCF degradation compared to 10.02% by sonolysis within 120 min of reaction duration. The low DCF degradation efficiency using US is understandable due to the low US frequency

(30 kHz) adopted in the current method which produces a small number of cavitation bubbles and results in low performance [8]. Combining photolysis and US enhanced the DCF degradation efficiency to 26.16%. Such a combination has been reported previously, where the improved performance is due to the synergistic effect of light and US radiation [42].

Combining the US with TiO₂ (US+TiO₂) was expected to increase the DCF degradation efficiency because the presence of pores on the surface of the photocatalyst can act as cavitation nuclei (nucleation) leading to growth (expansion), and finally the adiabatic implosion of cavitation bubbles promoting the degradation of pollutants [43]. However, the US+TiO₂ only achieved 23.18% DCF degradation which was lower than sonophotolysis (visible light + US = 26.16%), which could be attributed to lower cavitation activity triggered by the scattering of acoustic waves by the solid particles [11]. The lower DCF degradation efficiency by US + TiO₂ can also be due to the slower formation of degradation byproducts which reduce the cavitation activity following the addition of TiO₂ [8].

On the other hand, the DCF degradation efficiency was drastically enhanced to 52.87% by photocatalysis (visible light + TiO₂) within 120 min of reaction. The higher DCF removal via photocatalysis can be attributed to the exceptional flower-shaped morphology of the micro-sized materials which provides more active sites on the TiO₂ photocatalyst surface available for DCF adsorption, promotes visible light absorption, and transfers the charge carriers to the surface for photocatalytic reaction leading to the removal of DCF [33]. Combining US with photocatalysis (sonophotocatalysis) resulted in the highest DCF degradation of 62.61% in 120 min of visible light irradiation, which is in good agreement with previous studies [44]. The synergistic response of combining US + TiO₂ + visible light (sonophotocatalysis) could be explained as follows: the MST, with a relatively higher surface area, offers more chances for DCF adsorption; the visible light excites the electrons from the valence band of TiO₂ producing holes which may react with water to produce •OH radicals [44] which attack the DCF molecules.

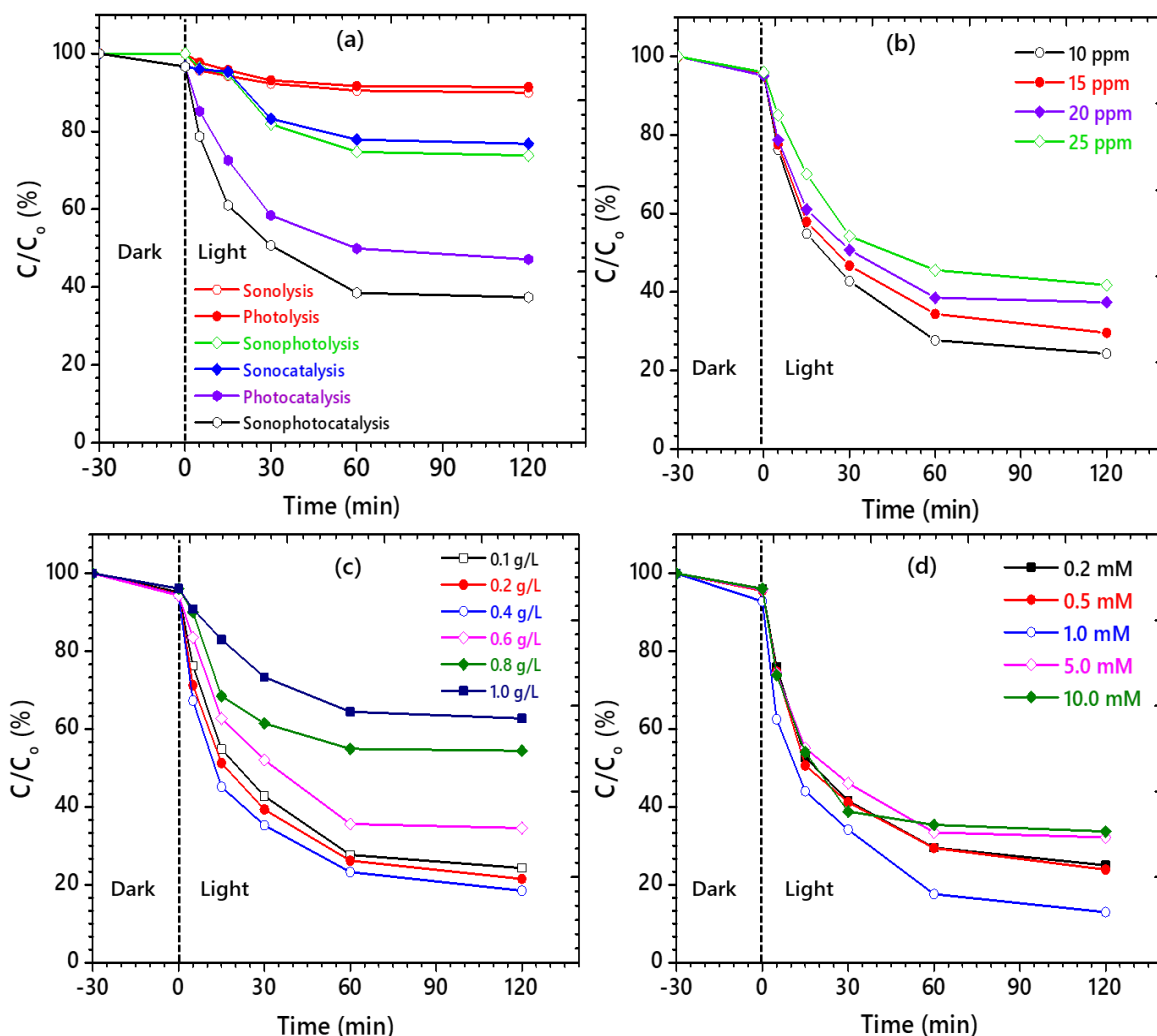


Figure 5. DCF degradation efficiencies, effect of (a) AOPs ($C_0=20$ ppm, 0.1 g/L of photocatalyst loading, and US frequency of 30 kHz), (b) initial concentration (0.1 g/L of photocatalyst loading and US frequency of 30 kHz), (c) photocatalyst loading (US frequency of 30 kHz, $C_0=10$ ppm), and (d) concentration of H₂O₂ dosage (0.4 g/L of photocatalyst loading, $C_0=10$ ppm, and US frequency of 30 kHz).

The US cavitation promotes the generation of more •OH radicals [45], which will eventually promote the degradation of DCF. In addition, US helps to continuously regenerate the TiO₂ photocatalyst surface exposing the active sites for DCF adsorption and subsequent degradation. When TiO₂ was irradiated with visible light in the presence of US, DCF molecules were oxidized by free radicals generated by the excited electrons and holes on TiO₂, and US splitting of H₂O molecules, as shown in Eqs. 3–6 [46, 47]:



Hence visible light-mediated photocatalysis coupled with US cavitation can be a new approach for DCF degradation in an aqueous environment. Since the DCF degradation efficiency of sonophotocatalysis was the highest amongst all the combinations of different AOPs, sonophotocatalytic treatment was further investigated for DCF degradation, and the effects of various research parameters such as initial concentration of DCF, photocatalyst loading and concentration of H₂O₂ dosage were considered.

3. Sonophotocatalytic Degradation of DCF

3.1. Effect of Initial Concentration of DCF

The sonophotocatalytic degradation performance was investigated at different initial concentrations of DCF (10, 15, 20, and 25 ppm) using 0.1 g/L of MST loading. Figure 5(b) shows that the initial DCF concentration has a significant effect on its degradation efficiency, achieving steady state after 60 min of reaction. The DCF degradation was highest, 75.69%, with 10 ppm initial concentration but the performance decreased as the initial concentration increased, giving only 58.23% degradation with 25 ppm. The amount of DCF degraded at 10 ppm initial DCF concentration was 7.57 ppm. If the initial DCF concentration was increased by a factor of 2.5 to 25 ppm, the amount degraded is estimated to be 18.92 ppm. However, from the experiment, the degradation of DCF at 25 ppm initial concentration was 14.56 ppm, which was 76.9% of the performance capacity at 10 ppm. The most probable explanation for the decrease in DCF degradation with increase in initial concentration may be the shielding effect of higher levels of DCF in the suspension, which could be responsible for the decrease in light absorption by the MST photocatalyst and subsequently the lower amount of hydroxyl radicals available for the degradation of the target pollutants [48]. Another probable explanation for the decrease in DCF degradation with increase in initial concentration may

be related to the active sites on the MST photocatalyst surface being covered by intermediate byproducts, making the surface area inaccessible for DCF adsorption and subsequent degradation [49]. Since a 10 ppm initial concentration of DCF showed the most promising performance capacity for DCF degradation, it was selected for further investigation.

3.2. Effect of Micron-sized TiO₂ Photocatalyst Loading

The effect of photocatalyst loading on DCF degradation was investigated with six different MST loadings (0.1, 0.2, 0.4, 0.6, 0.8, and 1.0 g/L) and the results are shown in Figure 5(c). The DCF degradation efficiency showed an increasing trend with increase in MST loading from 0.1–0.4 g/L, with the highest DCF degradation of 81.50% for 0.4 g/L loading within 120 min. This can be attributed to the higher number of active sites available for DCF adsorption and the simultaneous increase in the number of hydroxyl radicals and subsequent degradation [50]. However, the performance deteriorated with further increases in the photocatalyst loading showing a mere 37.24% degradation at 1.0 g/L. There may be several reasons for the reduction in performance with increasing MST photocatalyst loading: (i) excessive photocatalyst concentration causes the agglomeration of particles, thus reducing the available surface area for adsorption of DCF molecules [51]; (ii) high photocatalyst loading decreases the number of photons reaching the photocatalyst surface due to light attenuation [52] and/or scattering by solid nanoparticles [53]; and (iii) increased photocatalyst loading causes turbidity of the solution even in the presence of US [54, 55]. To ensure efficient absorption of photons and to avoid excess photocatalyst loading, the photocatalytic reaction should be operated at the optimum photocatalyst loading of 0.4 g/L for efficient degradation of DCF by the sonophotocatalytic process.

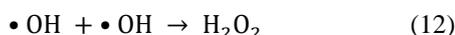
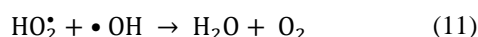
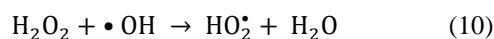
3.3. Effect of H₂O₂ Dosage

The effect of H₂O₂ dosage on DCF degradation efficiency was investigated using five different dosages: 0.2, 0.5, 1.0, 5.0, and 10.0 mM. The obtained results revealed that DCF degradation efficiency marginally increased with the addition of H₂O₂ as shown in Figure 5(d). For example, DCF degradation efficiency increased to 86.92% at 1.0 mM of H₂O₂ dosage in 120 min of visible irradiation, while in the absence of H₂O₂ the DCF degradation was 81.50%. Hydrogen peroxide plays a dual-role in photocatalytic reactions: firstly, H₂O₂ reduces the possibility of electron-hole pair recombination by trapping the electrons in the conduction band of TiO₂ [56, 57]; secondly, •OH free radicals are produced when H₂O₂ is supplemented by an energy dissipating source such as UV/visible light. These •OH radicals may react with H₂O₂ to form other free radical species which attack the pollutant molecules [58]. H₂O₂ can absorb

light energy from irradiation causing the HO–OH bond to be ruptured, leading to the production of reactive •OH. The mechanism involving H₂O₂ during TiO₂ photocatalysis can be explained using Eqs. 7–9 [57]:



As can be observed from Figure 5(d), the DCF degradation efficiency decreased when the concentration of H₂O₂ was increased to more than 1.0 mM. This may be due to the scavenging effect of H₂O₂ that reduces the degradation rate of DCF. The scavenging effect from higher concentrations of H₂O₂ can be explained in Eqs. 10–12. The hydroxyl radicals react with excess H₂O₂ producing peroxy radicals (Eq. 10) which consume the •OH radicals (Eq. 11). Subsequently, the •OH radicals produced in high amount dimerize back to H₂O₂ (Eq. 12) [59].



4. Performance of micron-sized and Nano-sized TiO₂ particles

Sonophotocatalytic reactions under the optimized conditions of 0.4 g/L of photocatalyst loading, 10 ppm initial DCF concentration, 30 kHz ultrasound frequency and 1.0 mM of H₂O₂ were carried out to evaluate and compare the performance of micron-sized and nano-sized TiO₂ for DCF degradation. Figure 6 shows that the MST displayed better performance by degrading 86.92% of DCF within the initial stage (60 min) of visible light irradiation, compared to only 53.24% by nano-sized TiO₂. The higher photocatalytic oxidation of DCF by MST can be attributed to its special flower-shaped morphology which provides more active sites on its surface for DCF adsorption. In addition, MST displayed better visible light absorption as well as a narrower bandgap (2.71 eV compared to 2.96 eV for nanomaterials), therefore a higher density of photogenerated charge carriers were transferred to the surface of the photocatalyst. It has been reported that special morphology such as rods, pompons, spindles, flower shapes, and dumbbell shapes can strongly affect the performance of a photocatalyst. For instance, Wong et al. [33] reported that ZnO with pompon-like morphology led to a higher COD removal efficiency of 96.0% from treated palm oil mill effluent compared to other morphologies including rod-like (43.0%), spindle-like (56.9%) and spherical-shaped (46.6%) structures. On the other hand, nanoflower morphology has been reported to exhibit a high surface area to volume ratio and efficient photocatalytic performance for dye degradation [60].

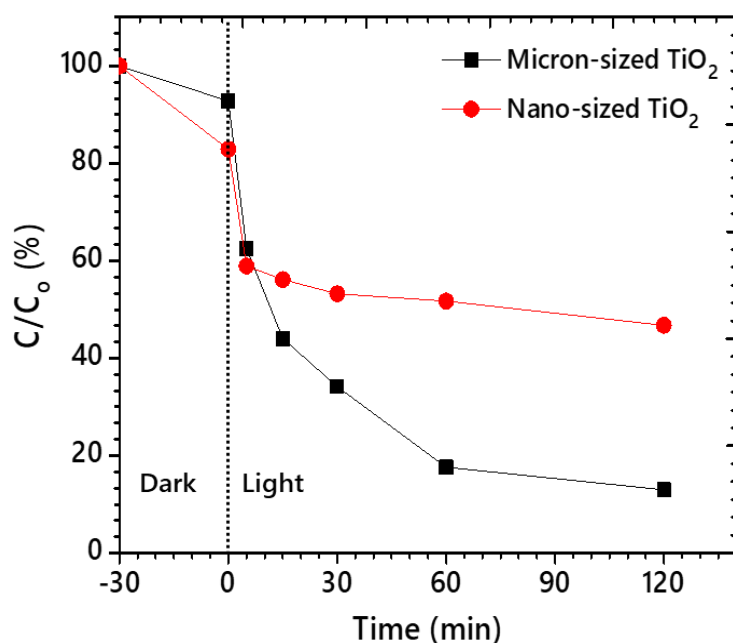


Figure 6. Performance of MST and nano-sized TiO₂ under the optimized conditions of 0.4 g/L photocatalyst loading, 10 ppm initial DCF concentration, and 1.0 mM H₂O₂ dosage.

Theoretically, the nano-sized TiO₂ particles could provide a larger active surface area to trigger enhanced photocatalytic oxidation of organic compounds. However, this does not imply the impossibility a priori of using MST in selected conditions [13]. In the present study, the better performance of the MST over nano-sized TiO₂ particles could be mainly due to better visible light absorption and a narrower bandgap of MST compared to nano-sized TiO₂ particles as evident from Figure 4(b) which facilitates easier electron-hole pair separation. The overall performance and photoactivity of TiO₂ can be strongly affected by the amount and duration of excited charges on its surface. The number of charge carriers is dependent on photon absorption. The more photons absorbed by TiO₂, the more working electrons and holes are likely to be available on the surface for photocatalytic reactions [61]. The comparatively wider bandgap of nano-sized TiO₂ (2.96 eV) has led to its lower photon absorption efficiency whereas the narrower bandgap of the MST (2.71 eV) makes it possible to display higher photon absorption efficiency and subsequent higher performance in the photodegradation of DCF. Another possible reason for the lower performance of nano-sized TiO₂ could be the excessive adsorption of DCF molecules on its surface, which blocks the active sites from further adsorption and subsequent degradation. It is evident from Figure 6 that almost 18% of DCF was adsorbed by nano-sized TiO₂ within the 30 min dark phase compared to only 8% by MST. Furthermore, the degradation of DCF by nano-sized TiO₂ was rapid at the initial stage but achieved steady state within 30 min of irradiation time, indicating

rapid deactivation.

5. Kinetics Studies and Synergy Index

The sonophotocatalytic results from DCF degradation were fitted to the pseudo-first order kinetic model represented by Eq. 13:

$$\ln \frac{C_o}{C_t} = kt \tag{13}$$

where C_o and C_t are the initial concentration and concentration of DCF at time (t), respectively and k represents the apparent rate constant for the pseudo-first order reaction.

The pseudo first order kinetic plots for all the AOPs showed good linearity as depicted in Figure 7. The rate of degradation showed an increasing trend from photolysis < sonolysis < sonocatalysis < sonophotolysis < photocatalysis < sonophotocatalysis. The linear regression and apparent rate constants obtained from the plots in Figure 7 are summarized in Table 3. Sonophotocatalytic degradation of DCF showed the largest rate constant value ($k = 0.0084 \text{ min}^{-1}$) where the degradation rate for sonophotocatalysis in the presence of MST photocatalyst was nearly two-fold compared to photocatalysis ($k = 0.0047 \text{ min}^{-1}$). This is probably due to the combination of AOPs in which the US cavitation not only enhances the generation of reactive $\bullet\text{OH}$, it contributes to constantly replenishing the available active sites on TiO₂ surface for adsorption of DCF or other surface reactions [11].

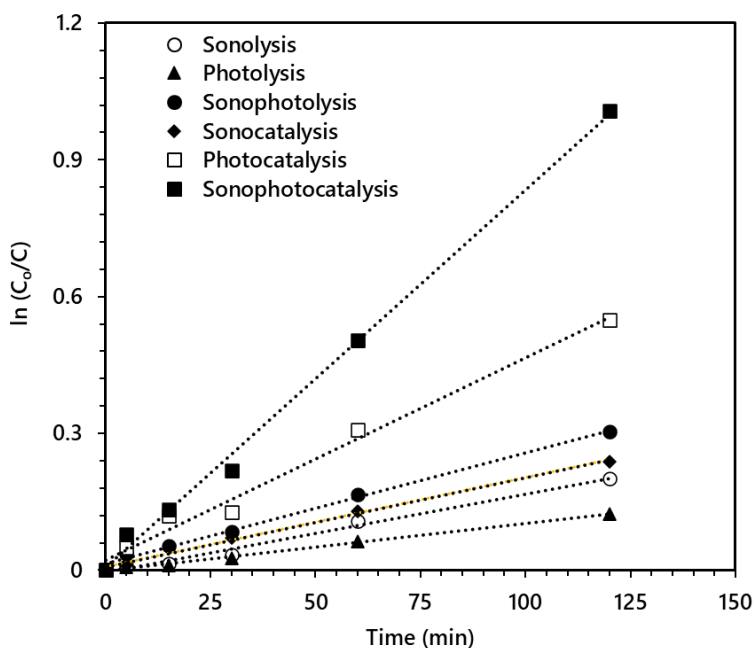


Figure 7. Pseudo first-order kinetics plots of DCF degradation by various AOPs conducted in ultrapure water (US frequency of 30 kHz, DCF initial concentration of 20 ppm and MST photocatalyst loading of 0.1 g/L).

Table 3. Rate constants of the Pseudo-first order kinetic model and synergy index for degradation of DCF via different AOPs.

AOP Processes	Apparent rate constant, k (min ⁻¹)	Regression (R ²)	Synergy index
Sonolysis	0.0017	0.9919	—
Photolysis	0.0010	0.9979	—
Sonophotolysis	0.0026	0.9923	0.9630
Sonocatalysis	0.0020	0.9942	—
Photocatalysis	0.0047	0.9900	—
Sonophotocatalysis	0.0084	0.9981	1.2537

By analyzing the rate constants displayed in Table 3, the synergistic effect of the two combined AOPs was estimated. The synergy indices (SI) of combined processes were calculated based on Eqs. 14 and 15. Based on the apparent rate constant values, the SI value of 1.25 was estimated for DCF degradation by photocatalysis assisted by US (sonophotocatalysis) using MST photocatalyst. An SI value higher than 1 indicates that the combined reaction (sonophotocatalysis) exceeds the sum of the separate reactions (sonolysis and photocatalysis). This is probably due to the increased amount of hydroxyl radicals during the degradation reaction and improved mass transfer of diclofenac between the bulk solution and photocatalyst surface [62]. US cavitation from the US processor de-aggregates the photocatalyst particles and increases the surface area accessible to DCF adsorption [63].

The SI value obtained in the present work barely compares with the value (2.20) for sonophotocatalytic degradation of DCF reported in the literature [8]. However, it is important to note that the previous study employed ultraviolet light instead of visible light which might be a reason for the higher SI value (2.20) for DCF degradation using a sonophotocatalytic process. It is well

documented that UV light drives higher degradation rates compared to visible light, especially with reference to •OH production. There is clearly a tradeoff between the SI and other considerations such as in the current study where visible light was used, providing the option of harvesting the visible light from free and abundant sunlight. On the hand, the SI values of 1.43 [64] and 1.3 [11] were reported in other studies using hydrodynamic cavitation and nanosized TiO₂ and P25, respectively employing 213 kHz sonication. In the present work, the degradation reactions were conducted using low US frequency of 30 kHz.

6. Mechanism of DCF degradation

The general photocatalytic degradation mechanism of DCF by photocatalysis is shown in Figure 8(a). Upon visible light irradiation, the electrons in the valence band of MST transfer to the conduction band. The photoexcited electrons reacts with the dissolved oxygen to produce reactive oxygen (O₂^{-•}) which further converts to •OH radicals. On the other hand, photogenerated holes in the valence band react with surface-adsorbed water or OH⁻ to produce •OH radicals [61] which are involved in the photooxidation of DCF.

$$SI(\text{sonophotolysis}) = \frac{k(\text{sonophotolysis})}{k(\text{sonolysis}) + k(\text{photolysis})} \quad (14)$$

$$SI(\text{sonophotocatalysis}) = \frac{k(\text{sonophotocatalysis})}{k(\text{sonocatalysis}) + k(\text{photocatalysis})} \quad (15)$$

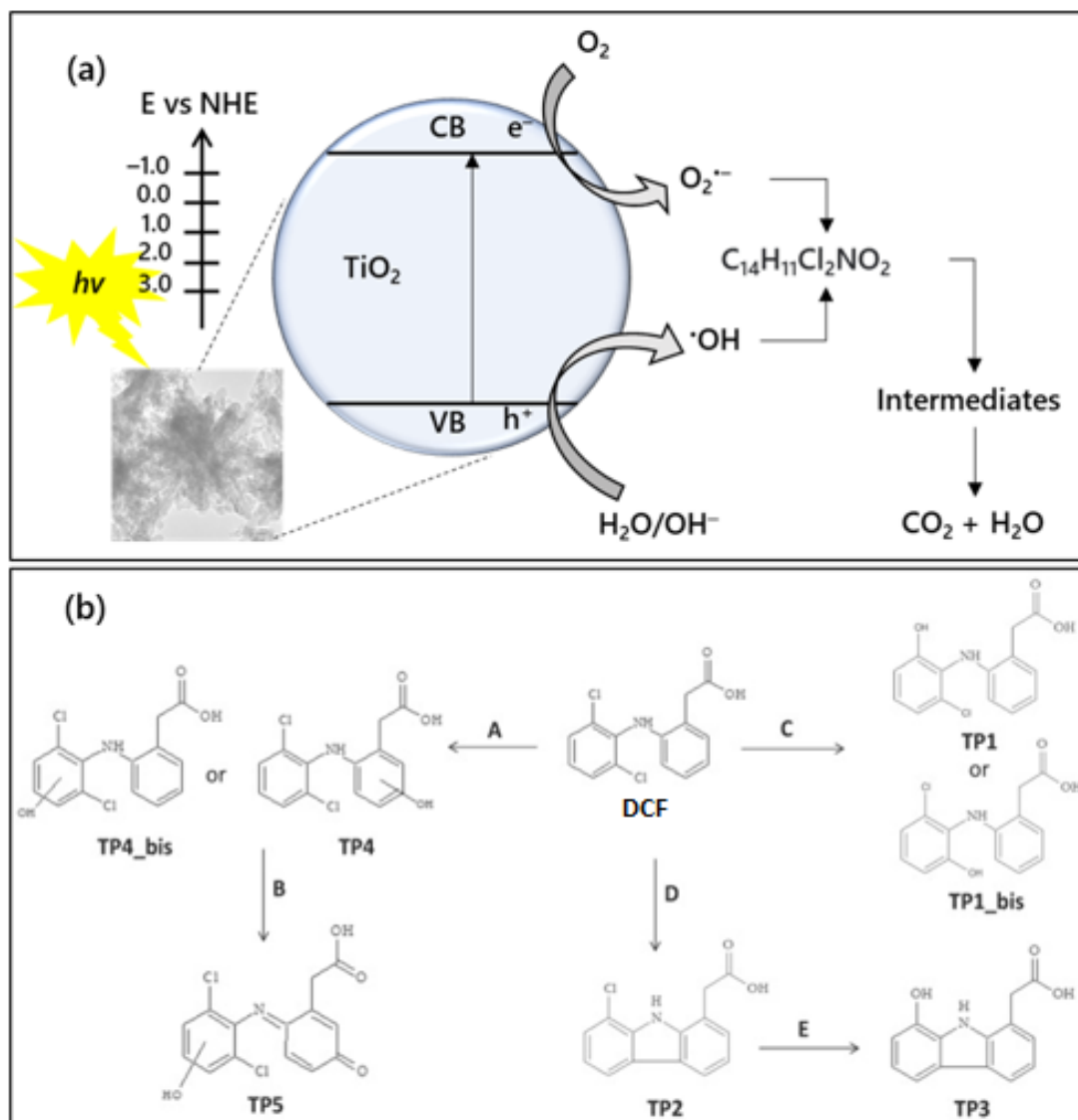


Figure 8. (a) Proposed degradation pathway and (b) transformational products of DCF degradation [8].

According to Meroni et al. [8], the photocatalytic and sonophotocatalytic degradation of DCF proceeds via the main pathway as shown in Figure 8(b). The same degradation pathway is proposed for the photocatalytic and sonophotocatalytic degradation of DCF in this work. Oxidation is the major reaction mechanism, as confirmed by the presence of transformational products (TP1 and TP4) [65]. In particular, $\cdot\text{OH}$ radicals appear to play a key role, which supports the proposed mechanism of synergistic effects from sonolysis and photocatalysis. The TP4 and TP4_{bis} species were most likely the results from the addition of $\cdot\text{OH}$ radicals to the aromatic rings (pathway A), whereas TP1 and TP1_{bis} could occur via the displacement of a chlorine substituent by a hydroxyl radical (pathway C). It is noteworthy that during sonolysis, the only intermediate detected in appreciable amounts was TP4, which supports a reaction mechanism driven by cavitation-generated hydroxyl radicals. However, TP4 was not appreciable during photolysis.

Amongst the other transformation products detected during photocatalytic and sonophotocatalytic reactions, TP5 presents two hydrogen atoms less than TP4, supporting the formation of benzoquinone imine (pathway B), in agreement with the literature [66]. The TP2 species could result from the loss of a chlorine substituent in DCF, leading to the formation of a carbazole ring by cyclization (pathway D). The displacement of the remaining chlorine atom in the TP2 species by a hydroxyl radical may be responsible for TP3 formation, as supported by an 18 Da mass decrease from TP2 to TP3 (pathway E).

7. Recycling of the Micron-sized TiO₂ Photocatalyst

The performance of the MST in three consecutive cycles is presented in Figure 9. It was noted that the performance of the photocatalyst decreased with each repeating cycle, from 86.46% to 83.63% and finally to 81.26%. The decrease in photocatalytic activity could be due to loss of photocatalyst material during recovery.

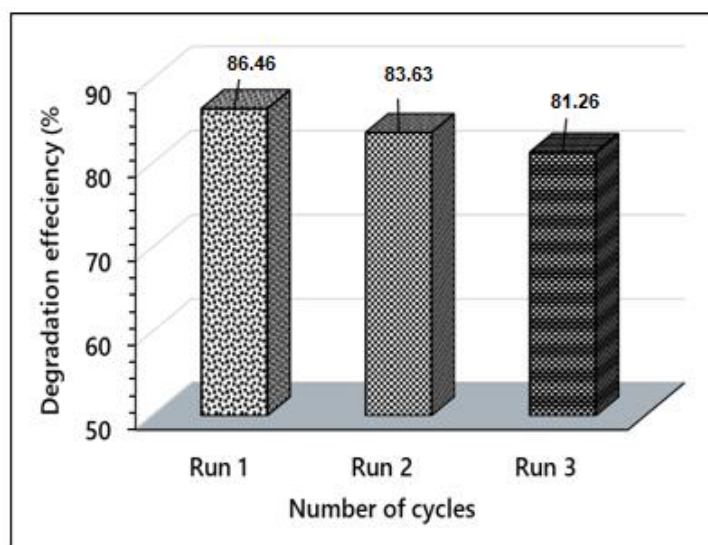


Figure 9. Performance of the MST photocatalyst for DCF degradation in three consecutive cycles.

There is a possibility that the reduction in degradation efficiency may be attributed to the reduction in number of active sites on the photocatalyst surface due to fouling. However, the MST photocatalyst was significantly stable under the employed process conditions with only a 5.19% decrease in performance after three consecutive cycles. In short, MST photocatalysts can be considered for industrial-scale applications in pharmaceutical wastewater treatment, especially when it can be activated by visible light and supported by ultrasonication.

CONCLUSION

Micron-sized TiO₂ with a particle size of 1.577 μm , surface area of 100.18 m^2/g and bandgap energy of 2.71 eV was successfully synthesized in this work. The DCF degradation efficiency from sonophotocatalysis was strongly affected by its initial concentration and the most promising performance capacity for DCF degradation was obtained at 10 ppm initial concentration. This was attributed to the synergistic effect of the combined processes confirmed by the synergy index of > 1 . The highest performance was achieved (81.50%) at 0.4 g/L TiO₂ loading. A further increase in the DCF degradation efficiency was observed when 1.0 mM of H₂O₂ was added to the system. Overall, the results revealed that visible light-driven photocatalysis in combination with US cavitation assisted by the presence of hydrogen peroxide (visible light + TiO₂ + US + H₂O₂) was the most efficient (86.92%) when conducted at the optimal conditions of 10 ppm initial concentration of DCF, 0.4 g/L of MST photocatalyst loading, 1.0 mM of H₂O₂ dosage and 30 kHz of US frequency in 120 min of visible light irradiation. Kinetic analysis of the data obtained showed that sonophotocatalytic degradation of DCF followed pseudo-first order kinetics with a rate constant of 0.0084 min^{-1} . The recyclability tests indicated that the MST

photocatalyst could be easily recovered via centrifugation after the treatment and reused repeatedly for several consecutive runs with minimal depletion in performance. The visible light driven photocatalysis based on a flower-like MST photocatalyst coupled with US cavitation and addition of H₂O₂ is a promising approach for remediation of pharmaceutical waste effluent containing DCF. The combined approach adopted in this study shows that MST is a viable alternative in terms of energy consumption and environmental impact compared to nano-sized TiO₂.

ACKNOWLEDGMENTS

The authors would like to thank the Centre of Innovative Nanostructures and Nanodevices (COINN), and Photocatalyst Laboratory at Catalyst Research (CARE) Laboratory in Universiti Teknologi PETRONAS for providing the facilities. Financial support from the Ministry of Higher Education Malaysia (FRGS/1/2020/STG05/UTP/02/2) and from Yayasan Universiti Teknologi PETRONAS (YUTP 015LC0-276) are gratefully acknowledged.

REFERENCES

1. Scheurell, M., Franke, S., Shah, R. M. and Huhnerfuss, H. (2009) Occurrence of diclofenac and its metabolites in surface water and effluent samples from Karachi, Pakistan. *Chemosphere*, **6**, 870–876.
2. Stulten, D., Zuhlke, S., Lamshoft, M. and Spittler, M. (2008) Occurrence of diclofenac and selected metabolites in sewage effluents. *Science of The Total Environment*, **1**, 310–316.
3. Facey, S. J., Nebel, B. A., Kontny, L., Allgaier, M. and Hauer, B. (2018) Rapid and complete degradation of diclofenac by native soil

- microorganisms. *Environmental Technology & Innovation*, **10**, 55–61.
- Triebkorn, R., Casper, H., Heyd, A., Eikemper, R., Kohler, H. R. and Schwaiger, J. (2004) Toxic effects of the non-steroidal anti-inflammatory drug diclofenac: Part II. Cytological effects in liver, kidney, gills and intestine of rainbow trout (*Oncorhynchus mykiss*). *Aquatic Toxicology*, **2**, 151–166.
 - Oaks, J. L., Gilbert, M., Virani, M. Z., Watson, R. T., Meteyer, C. U., Rideout, B. A., Shivaprasad, H. L., Ahmed, S., Chaudhry, M. J., Arshad, M. and Mahmood, S. (2004) Diclofenac residues as the cause of vulture population decline in Pakistan. *Nature*, **6975**, 630–633.
 - Maryam, B., Buscio, V., Odabasi, S. U. and Buyukgungor, H. (2020) A study on behavior, interaction and rejection of Paracetamol, Diclofenac and Ibuprofen (PhACs) from wastewater by nanofiltration membranes. *Environmental Technology & Innovation*, **18**, 100641.
 - Rozas, O., Vidal, C., Baeza, C., Jardim, W. F., Rossner, A. and Mansilla, H. D. (2016) Organic micropollutants (OMPs) in natural waters: oxidation by UV/H₂O₂ treatment and toxicity assessment. *Water Research*, **98**, 109–118.
 - Meroni, D., Jimenez-Salcedo, M., Falletta, E., Bresolin, B. M., Kait, C. F., Boffito, D. C., Bianchi, C. L. and Pirola, C. (2020) Sonophotocatalytic degradation of sodium diclofenac using low power ultrasound and micro sized TiO₂. *Ultrasonics Sonochemistry*, **67**, 105123.
 - Al-Bsoul, A., Al-Shannag, M., Tawalbeh, M., Al-Taani, A. A., Lafi, W. K., Al-Othman, A. and Alsheyab, A. (2020) Optimal conditions for olive mill wastewater treatment using ultrasound and advanced oxidation processes. *Science of The Total Environment*, **700**, 134576.
 - Schieppati, D., Galli, F., Peyot, M. L., Yargeau, V., Bianchi, C. L. and Boffito, D. C., (2019) An ultrasound-assisted photocatalytic treatment to remove an herbicidal pollutant from wastewaters. *Ultrasonics Sonochemistry*, **54**, 302–310.
 - Madhavan, J., Kumar, P. S., Anandan, S., Zhou, M., Grieser, F. and Ashokkumar, M. (2010) Ultrasound assisted photocatalytic degradation of diclofenac in an aqueous environment. *Chemosphere*, **80**, 747–752.
 - Samal, A. and Das, D. P. (2018) Transfiguring UV light active “metal oxides” to visible light active photocatalyst by reduced graphene oxide hypostatization. *Catalysis Today*, **300**, 124–135.
 - Kwon, S. Fan, Cooper, M. A. T. and Yang, H. (2018) Photocatalytic applications of micro- and nano-TiO₂ in environmental engineering. *Critical Reviews in Environmental Science and Technology*, **38**, 197–226.
 - Zangeneh, H., Zinatizadeh, A., Habibi, M., Akia, M. and Isa, M. H. (2015) Photocatalytic oxidation of organic dyes and pollutants in wastewater using different modified titanium dioxides: A comparative review. *Journal of Industrial Engineering Chemistry*, **26**, 1–36.
 - Clement, L., Hurel, C. and Marmier. (2013) Toxicity of TiO₂ nanoparticles to cladocerans, algae, rotifers and plants—Effects of size and crystalline structure. *Chemosphere*, **90**, 1083–1090.
 - Baranowska-Wojcik, E., Szwajgier, D., Oleszczuk, P. and Winiarska-Mieczan, A. (2020) Effects of titanium dioxide nanoparticles exposure on human health—a review. *Biological Trace Element Research*, **193**, 118–129.
 - Bianchi, C. L., Gatto, S., Pirola, C., Naldoni, A., Di Michele, A., Cerrato, G., Crocella, V. and Capucci, V. (2014) Photocatalytic degradation of acetone, acetaldehyde and toluene in gas-phase: Comparison between nano and micro-sized TiO₂. *Applied Catalysis B: Environmental*, **146**, 123–130.
 - Velazquez-Martinez, S., Silva-Martinez, S., Pineda-Arellano, C. A., Jimenez-Gonzalez, A., Salgado-Transito, I., Morales-Perez, A. A., and Pena-Cruz, M. I. (2018) Modified sol-gel/hydrothermal method for the synthesis of micro-sized TiO₂ and iron-doped TiO₂, its characterization and solar photocatalytic activity for an azo dye degradation. *Journal of Photochemistry and Photobiology A: Chemistry*, **359**, 93–101.
 - Zhao, Q. E., Wen, W., Xia, Y., and Wu J. M. (2018) Photocatalytic activity of TiO₂ nanorods, nanowires and nanoflowers filled with TiO₂ nanoparticles. *Thin Solid Films*, **648**, 103–107.
 - Kim, D. S. and Kwak, S. Y. (2007) The hydrothermal synthesis of mesoporous TiO₂ with high crystallinity, thermal stability, large surface area, and enhanced photocatalytic activity. *Applied Catalysis A: General*, **323**, 110–118.
 - Zhang, D., Lee, C., Javed, H., Yu, P., Kim, J. H., and Alvarez, P. J. Easily recoverable, micrometer-sized TiO₂ hierarchical spheres

- decorated with cyclodextrin for enhanced photocatalytic degradation of organic micropollutants. *Environmental Science & Technology*, **52**, 12402–12411.
22. Zheng, Z., Huang, B., Qin, X., Zhang, X. and Dai, Y. (2010) Strategic synthesis of hierarchical TiO₂ microspheres with enhanced photocatalytic activity. *Chemistry–A European Journal*, **16**, 11266–11270.
 23. Xiang, L., Zhao, X., Yin, J. and Fan, B. (2012) Well-organized 3D urchin-like hierarchical TiO₂ microspheres with high photocatalytic activity. *Journal of Materials Science*, **47**, 1436–1445.
 24. Nawaz, R., Kait, C. F., Chia, H. Y., Isa, M. H. and Huei, L. W. (2019) Glycerol-mediated facile synthesis of colored titania nanoparticles for visible light photodegradation of phenolic compounds. *Nanomaterials*, **9**, 1586.
 25. Jitputti, J., Suzuki, Y. and Yoshikawa, S. (2008) Synthesis of TiO₂ nanowires and their photocatalytic activity for hydrogen evolution. *Catalysis Communications*, **9**, 1265–1271.
 26. Mugunthan, E., Saidutta, M. B. and Jagadeeshbabu, P. E. (2018) Visible light assisted photocatalytic degradation of diclofenac using TiO₂-WO₃ mixed oxide catalysts. *Environmental Nanotechnology, Monitoring & Management*, **10**, 322–330.
 27. Nie, E., Yang, M., Wang, D., Yang, X., Luo, X. and Zheng, Z. (2014) Degradation of diclofenac by ultrasonic irradiation: kinetic studies and degradation pathways. *Chemosphere*, **113**, 165–170.
 28. Li, J. G., Ishigaki, T. and Sun, X. (2007) Anatase, brookite, and rutile nanocrystals via redox reactions under mild hydrothermal conditions: phase-selective synthesis and physicochemical properties. *The Journal of Physical Chemistry C*, **111**, 4969–4976.
 29. Tsang, C. H., Li, K., Zeng, Y., Zhao, W., Zhang, T., Zhan, Y., Xie, R., Leung, D. Y. and Huang, H. (2019) Titanium oxide based photocatalytic materials development and their role in the air pollutants degradation: Overview and forecast. *Environment International*, **125**, 200–228.
 30. Fischer, K., Gawel, A., Rosen, Krause, M., Abdul Latif, A., Griebel, J., Prager, A. and Schulze, A. (2017) Low-temperature synthesis of anatase/rutile/brookite TiO₂ nanoparticles on a polymer membrane for photocatalysis. *Catalysts*, **7**, 209.
 31. Yahaya, M. Z., Azam, M. A., Teridi, M. A., Singh, P. K. and Mohamad, A. A. (2017) Recent Characterisation of Sol-Gel Synthesised TiO₂ Nanoparticles, in *Recent Applications in Sol-Gel Synthesis*, InTechOpen, London, United Kingdom.
 32. Chen, X., Liu, L. and Huang, F. (2015) Black titanium dioxide (TiO₂) nanomaterials. *Journal of Chemical Society Reviews*, **44**, 1861–1885.
 33. Wong, K. A., Lam, S. M. and Sin, J. C. (2019) Wet chemically synthesized ZnO structures for photodegradation of pre-treated palm oil mill effluent and antibacterial activity. *Ceramics International*, **45**, 1868–1880.
 34. Nawaz, R., Kait, C. F., Chia, H. Y., Isa, M. H. and Huei, L. W. (2020) Photocatalytic remediation of treated palm oil mill effluent contaminated with phenolic compounds using TiO₂ nanomaterial. *Desalination and Water Treatment*, **183**, 355–365.
 35. Wei, J., Yao, J., Zhang, X., Zhu, W., Wang, H., Rhodes, M. H. (2007) Hydrothermal growth of titania nanostructures with tunable phase and shape. *Materials Letters*, **61**, 4610–4613.
 36. Liu, G., Yang, H. G., Sun, C., Cheng, L., Wang, L., Lu, G. Q. and Cheng, H. M. (2009) Titania polymorphs derived from crystalline titanium diboride. *Cryst. Eng. Comm.*, **11**, 2677–2682.
 37. Wen, J., Li, X., Liu, W., Fang, F., Xie, J. and Xu, Y. (2015) Photocatalysis fundamentals and surface modification of TiO₂ nanomaterials. *Chinese Journal of Catalysis*, **36**, 2049–2070.
 38. Ren, T. Z., Yuan, Z. Y. and Su, B. L. (2003) Surfactant-assisted preparation of hollow microspheres of mesoporous TiO₂. *Chemical Physics Letters*, **374**, 170–175.
 39. Chen, Y. and Dionysiou, D. D. (2008) Bimodal mesoporous TiO₂-P25 composite thick films with high photocatalytic activity and improved structural integrity. *Applied Catalysis B: Environmental*, **80**, 147–155.
 40. Rasalingam, S., Wu, C. M. and Koodali, R. K. (2015) Modulation of pore sizes of titanium dioxide photocatalysts by a facile template free hydrothermal synthesis method: implications for photocatalytic degradation of rhodamine B. *ACS Applied Materials & Interfaces*, **7**, 4368–4380.
 41. Yang, P., Deng, T., Zhao, D., Feng, P., Pine, D., Chmelka, B. F., Whitesides, G. M. and Stucky, G. D. (1998) Hierarchically ordered oxides. *Science*, **282**, 2244–2246.
 42. Ghafoori, S., Mowla, A., Jahani, R., Mehrvar, M. and Chan, P. K. (2015) Sonophotolytic degradation of synthetic pharmaceutical

- wastewater: Statistical experimental design and modeling. *Journal of Environmental Management*, **150**, 128–137.
43. Hartmann, J., Bartels, P., Mau, U., Witter, M., Tumppling, W. V., Hofmann, J. and Nietzsche, E. (2008) Degradation of the drug diclofenac in water by sonolysis in presence of catalysts. *Chemosphere*, **70**, 453–461.
 44. Achilleos, A., Hapeshi, E., Xekoukoulotakis, N. P., Mantzavinos, D. and Fatta-Kassinos, D. (2010) Factors affecting diclofenac decomposition in water by UV-A/TiO₂ photocatalysis. *Chemical Engineering Journal*, **161**, 53–59.
 45. Mohajerani, M., Mehrvar, M., and Ein-Mozaffari, F. (2010) Recent achievements in combination of ultrasonolysis and other advanced oxidation processes for wastewater treatment. *International Journal of Chemical Reactor Engineering*, **8**, 2010.
 46. Ahmedchekkat, F., Medjram, M. S., Chiha, M. and Al-Bsoul, A. M. (2011) Sonophotocatalytic degradation of Rhodamine B using a novel reactor geometry: Effect of operating conditions. *Chemical Engineering Journal*, **178**, 244–251.
 47. Deepthi, S., Venkatesan, J., Kim, S. K., Bumgardner, J. D. and Jayakumar, R. (2016) An overview of chitin or chitosan/nano ceramic composite scaffolds for bone tissue engineering. *International Journal of Biological Macromolecules*, **93**, 1338–1353.
 48. David, B. (2009) Sonochemical degradation of PAH in aqueous solution. Part I: Monocomponent PAH solution. *Ultrasonics Sonochemistry*, **16**, 260–265.
 49. Yao, Y. (2016) Enhancement of mass transfer by ultrasound: Application to adsorbent regeneration and food drying/dehydration. *Ultrasonics Sonochemistry*, **31**, 512–531.
 50. Rizzo, L., Meric, S., Guida, M., Kassinos, D. and Belgiorno, V. (2009) Heterogeneous photocatalytic degradation kinetics and detoxification of an urban wastewater treatment plant effluent contaminated with pharmaceuticals. *Water Research*, **43**, 4070–4078.
 51. Eskandarloo, E., Badiei, A., Behnajady, M. A. and Ziarani, G. M. (2015) Ultrasonic-assisted sol-gel synthesis of samarium, cerium co-doped TiO₂ nanoparticles with enhanced sonocatalytic efficiency. *Ultrasonics Sonochemistry*, **26**, 281–292.
 52. Wong, C. and Chu, W. (2003) The direct photolysis and photocatalytic degradation of alachlor at different TiO₂ and UV sources. *Chemosphere*, **50**, 981–987.
 53. Brandi, R., Martin, C., Alfano, O. and Cassano, A. (2002) A Laboratory reactor for photocatalytic studies in slurry operation. *Journal of Advanced Oxidation Technologies*, **5**, 175–185.
 54. Pardeshi, S. and Patil, A. (2008) A simple route for photocatalytic degradation of phenol in aqueous zinc oxide suspension using solar energy. *Solar Energy*, **82**, 700–705.
 55. Neppolian, B., Ciceri, L., Bianchi, C. L., Grieser, F. and Ashokkumar, M. (2011) Sonophotocatalytic degradation of 4-chlorophenol using Bi₂O₃/TiZrO₄ as a visible light responsive photocatalyst. *Ultrasonic Sonochemistry*, **18**, 135–139.
 56. Eskandarloo, H., Badiei, A. and Behnajady, M. A. (2014) Study of the effect of additives on the photocatalytic degradation of a triphenylmethane dye in the presence of immobilized TiO₂/NiO nanoparticles: artificial neural network modeling. *Industrial & Engineering Chemistry Research*, **53**, 6881–6895.
 57. Tayade, R. J., Natarajan, T. S. and Bajaj, H. C. (2009) Photocatalytic degradation of methylene blue dye using ultraviolet light emitting diodes. *Industrial & Engineering Chemistry Research*, **48**, 10262–10267.
 58. Saien, J., Soleymani, A. and Sun, J. (2011) Parametric optimization of individual and hybridized AOPs of Fe²⁺/H₂O₂ and UV/S₂O₈²⁻ for rapid dye destruction in aqueous media. *Desalination*, **279**, 298–305.
 59. Liu, N., Sijak, S., Zheng, M., Tang, L., Xu, G. and Wu, M. (2015) Aquatic photolysis of florfenicol and thiamphenicol under direct UV irradiation, UV/H₂O₂ and UV/Fe(II) processes. *Chemical Engineering Journal*, **260**, 826–834.
 60. Sajid, M. M., Shad, N. A., Javed, Y., Khan, S. B., Zhang, Z., Amin, N. and Zhai, H. (2020) Morphological effects on the photocatalytic performance of FeVO₄ nanocomposite. *Nano-Structures & Nano-Objects*, **22**, 100431.
 61. Gaya, U. I. and Abdullah, A. H. (2008) Heterogeneous photocatalytic degradation of organic contaminants over titanium dioxide: a review of fundamentals, progress and problems. *Journal of Photochemistry and Photobiology C: Photochemistry Reviews*, **9**, 1–12.

- 125 Thamisha Steven, Rab Nawaz, Nurul Tasnim Sahrin, Kar Mun Lee, Claudia L. Bianchi and Chong Fai Kait
H₂O₂-assisted Sonophotocatalytic Degradation of Diclofenac using a Visible Light-Active Flower-like Micron-sized TiO₂ Photocatalyst
62. Michael, I., Achilleos, A., Lambropoulou, D., Torrens, V. O., Perez, S., Petrovic, M., Barcelo, D. and Fatta-Kassinos, D. (2014) Proposed transformation pathway and evolution profile of diclofenac and ibuprofen transformation products during (sono) photocatalysis. *Applied Catalysis B: Environmental*, **147**, 1015–1027.
63. Berberidou, C., Poullos, I., Xekoukoulotakis, N. P. and Mantzavinos, D. (2007) Sonolytic, photocatalytic and sonophotocatalytic degradation of malachite green in aqueous solutions. *Applied Catalysis B: Environmental*, **74**, 63–72.
64. Bagal, M. V. and Gogate, P. R. (2014) Degradation of diclofenac sodium using combined processes based on hydrodynamic cavitation and heterogeneous photocatalysis. *Ultrasonics Sonochemistry*, **21**, 1035–1043.
65. Murgolo, S., Moreira, I. S., Piccirillo, C., Castro, P. M., Ventrella, G., Cocozza, C. and Mascolo, G. (2018) Photocatalytic degradation of diclofenac by hydroxyapatite–TiO₂ composite material: Identification of transformation products and assessment of Toxicity. *Materials*, **11**, 1779.
66. Martinez, C., Fernandez, M. I., Santaballa, J. A. and Faria, J. (2011) Aqueous degradation of diclofenac by heterogeneous photocatalysis using nanostructured materials. *Applied Catalysis B: Environmental*, **107**, 110–118.